Asian Journal of Chemistry; Vol. 35, No. 12 (2023), 2899-2910

ASIAN JOURNAL OF CHEMISTRY

https://doi.org/10.14233/ajchem.2023.28277

Synthesis, Characterization, Dielectric and Antibacterial Studies of TiO_2-Phosphomolybdic Acid Nanocomposite

M. PRAVEEN DANIEL[1], P. RAJESH ANANTHA SELVAN[1,*] and D. PARAMANANTHA SWAMI DOSS[2]

[1]Department of Chemistry, St. John's College (Affiliated to Manonmaniam Sundaranar University, Tirunelveli), Palayamkottai-627002, India
[2]Department of Zoology, St. John's College (Affiliated to Manonmaniam Sundaranar University, Tirunelveli), Palayamkottai-627002, India

*Corresponding author: E-mail: rajesh.chem@stjohnscollege.edu.in

Received: 29 June 2023; *Accepted*: 8 August 2023; *Published online*: 2 December 2023; AJC-21448

In this work, the synthesis of TiO_2-phosphomolybdic acid nanocomposites was achieved by annealing method and characterized by UV-visible, FT-IR, XRD, EDAX and SEM. The UV-visible spectroscopy revealed a strong interaction between the TiO_2 and phosphomolybdic acid, while the FT-IR spectroscopy confirmed the presence of phosphomolybdic acid in the nanocomposite. Moreover, the X-ray diffraction (XRD) analysis revealed a decrease in the crystallite size of the nanocomposite materials. This finding was further supported by the SEM images, which exhibited a reduction in particle size and a uniform distribution of the dopant. The photocatalytic activity of the nanocomposite, the methylene blue dye degradation was used and the results proved a good catalytic activity (99.41%). The favourable results have been obtained by measuring the dielectric constants and analyzing the temperature dependence of AC and DC electrical conductivities of the composite materials. The antibacterial properties of the nanocomposites were also evaluated using the agar well diffusion method on *Streptococcus* pyogenes, exhibiting the significant results. Overall, the synthesized TiO_2-phosphomolybdic acid nanocomposites have proven as promising composites in various studies, suggesting their potential applications in many different fields.

Keywords: Phosphomolybdic acid, Nanocomposite, Dielectric studies, Antimicrobial activities.

INTRODUCTION

Nanocomposites represent a novel category of materials that are produced through the integration of nanoscale components with conventional polymeric materials. Nanoscale blending of two or more phases using polymers [1], metals or ceramics [2], results in the formation of novel materials with unique properties. These nanoscale building blocks result improved properties, such as mechanical strength, better thermal stability and enhanced electrical and optical properties [3]. Nanocomposites have a wide range of potential applications, such as in automotive, aerospace, electronics and medical fields. TiO_2 nanocomposites have potential applications in a sustainable environment. For example, nanocomposites can be used to improve the efficiency of solar cells and photovoltaic panels, which can help to reduce the reliance on fossil fuels and promote the use of renewable energy sources. TiO_2 nanocomposites can be used in water purification to reduce pollutants and contaminants, improving water quality and reducing the risk of waterborne diseases [4]. They are also used in air purification by absorbing volatile organic compounds, which can help to reduce air pollution [5].

Since nanocomposites are made up of non-traditional nanocomposite particles that interact with the environment and ultimately result in material behaviour, nanocomposite research must be able to withstand fundamental theories. Furthermore, the challenge exists to predict and control the structure-property relationship, in order to develop materials with enhanced properties. TiO_2 doped phosphomolybdic acid has the sustainable solution for the environment [6]. This innovative material is a photocatalyst that can be used to break down organic pollutants and hazardous compounds into harmless byproducts, reducing their impact on the environment. In addition, the material does not produce any hazardous byproducts, making it suitable for a wide range of applications. With its combination of properties, TiO_2 doped phosphomolybdic acid provides an excellent opportunity for a sustainable and greener future [7].

Heteropolyacids exhibit strong acidity and alternatively, exhibit suitable redox characteristics that can be controlled by altering the chemical composition of the heteropolyanion.

Thus, heteropolyacids are widely used as adsorbent, catalyst, photocatalyst, *etc*. [8,9]. TiO_2 doped phosphomolybdic acid (PMA) is a promising composite material for sustainable environmental applications, as it enhances the photostability and surface area of TiO_2, a semiconductor for photocatalytic degradation of organic pollutants [10]. PMA molecules form strong bonds with the TiO_2 surface, reducing electron-hole recombination and providing additional active sites. Moreover, this highlights the possibility of this composite material for sustainable environment applications, as it not only helps in organic pollutant degradation [11], but also shows its capacity in controlling the growth of harmful microorganisms [12]. The TiO_2-PMA nanocomposite which is a semiconductor with a wide bandgap, providing optical, electronic, magnetic, thermal, mechanical and chemical qualities [13]. Meanwhile, TiO_2 is eco-friendly, abundant and varying oxidation states and electrochemical reversibility that make it ideal for energy storage [14]. In this work, TiO_2 doped with various concentration of phosphomolybdic acid (PMA) were prepared by annealing method and characterized by means of UV-visible, FT-IR, XRD, EDAX and SEM techniques. The dielectrical properties and the antimicrobial activity of the samples were also studied.

EXPERIMENTAL

For the synthesis of TiO_2 nanocomposite and TiO_2-doped phosphomolybdic acid nanocomposite, analytical grade reagent such as TiO_2, phosphomolybdic acid, ethanol, double distilled water and methylene blue dye were procured from Merck, India. All the reagents were handled with standard laboratory protocols to ensure successful synthesis.

Synthesis of TiO_2 doped phosphomolybdic acid nanocomposite: The annealing method was used to synthesize pure TiO_2 and TiO_2 doped phosphomolybdic acid nanocomposite that involves mixing 1 g of TiO_2 with various concentrations of phosphomolybdic acid. Sample 2, 3, 4 and 5 were synthesized by enhancing PMA concentrations of 0.01 M, 0.001 M, 0.05 M and 0.005 M, respectively. The samples were annealed for 3 h at 300 ºC. During the annealing process, the TiO_2 composite in the mixture begins to grow and form a new nanocomposite with the phosphomolybdic acid. After completion, the nanocomposite samples were cooled at room temperature and grounded to powder.

Characterization: The UV-Vis spectra of the samples were measured by using the JascoV-600 spectrophotometer in the 200-900 nm wavelength range. To record the FTIR spectra, the Shimadzu 8400S model was used, while the Jasco 550 double beam spectrophotometer was used to capture the electronic spectra. The XRD patterns of the products were observed by using a Philips powder X-ray diffractometer (Model PW-1710) and operated at the rate of 2º min^{-1} with Cu*K*α X-ray radiation as source. The XRD patterns were recorded in the range of 10º-80º and the step size of 0.02º, utilizing Cu*K*α radiation with a wavelength of 1.5406 Å. The average bulk composition and size of the particles were calculated. The SEM with EDAX analysis was conducted by using a scanning electron microscope of the model, TESCAN VEGAS-3 and operated at the voltage of 20 kV. This method provided a detailed view of the samples being analyzed, giving insight into the composition and structure of the material at the microscopic level.

The optical band gap energy was calculated using eqn. 1:

$$E = (\alpha h\nu)^2 \text{ (eV cm}^{-1})^2 \textit{ vs.} \text{ Energy (eV)} \quad (1)$$

where h is the Planck's constant; c is the speed of light and ν is the frequency of the light incident.

The Urbach energy equation was used to calculate the optical absorption coefficient (α) of the material from the measured absorption edge (C) and the photon energy (hν) in electron volts (eV). The equation is given as follows:

$$\ln \alpha = \frac{\ln(C) - 1240}{h\nu} \quad (2)$$

Overall, the XRD analysis of TiO_2 doped phosphomolybdic acid nanocomposites suggests a stable crystal structure with incorporated dopants. It has been obtained from the following Scherrer's equation [15].

$$D = \frac{0.94\lambda}{\beta \cos\theta} \quad (3)$$

where λ is the X-ray wavelength, β is the full width at half maximum of the diffraction peak and θ is the Bragg angle.

The size of the nanocomposites can be calculated using the equation given below:

$$\text{Size (nm)} = \frac{0.94 \times \lambda}{(2 \times \beta \times \cos\theta)} \quad (4)$$

The Williamson-Hall plot method was used to analyze the crystallite size and strain of TiO_2-doped phosphomolybdic acid nanocomposite samples. Sample 1 was pure TiO_2, whereas samples 2 to 5 were TiO_2-doped phosphomolybdic acid nanocomposites. The *x*-axis in the plot corresponds to the sin θ value of the scattering angle, while the *y*-axis corresponds to the β cos θ values. Eqn. 5 was used for calculating the data points of the plot:

$$\beta \cos\theta = \varepsilon(4 \sin\theta) + \frac{\kappa\lambda}{D} \quad (5)$$

where ε is the strain, k is a constant, λ is the X-ray wavelength and D is the crystallite size of the sample.

The electrical properties of TiO_2 nanocomposites doped phosphomolybdic acid at 0.05 M concentration were assessed by using eqn. 6:

$$\varepsilon_r = \frac{2\pi Fcd}{A \tan\delta} \quad (6)$$

where ε_r is the dielectric constant; c is the capacitance; d is the distance and A is the area of sample, where the capacitance is determined by the frequency (F) of the signal and the loss tangent (tan δ).

The electrical response of TiO_2 and TiO_2 doped phosphomolybdic acid under applied electric field was measured by dielectric constant which can be calculated by the equation is:

$$\varepsilon_r = \frac{cd}{A\varepsilon_o} \quad (7)$$

The dielectric property of material is related to its electrical polarization and the permittivity of its environment. In this

case, the permittivity of the environment is the dielectric loss, which was calculated by using eqn. 8:

$$\tan\delta = \frac{\varepsilon_r}{\varepsilon_o} \quad (8)$$

Photocatalytic degradation activity: The photocatalytic degradation of methylene blue dye was studied using inner photocatalytic reactor. As prior to being placed in the reaction chamber, the dye solution mixed with the photocatalyst was aerated for 30 min in order to reach equilibrium. Following this, the solution was irradiated with light at 365 nm for 3 h. Samples of the dye solution were collected in intervals of 10, 20, 30, 40, 50, 60, 120 and 180 min to measure the breakdown. The sample dye solution (2 mL) was used to measure an optical density in a UV-vis spectrophotometer. The efficiency of the degradation process (η) was measured by comparing the initial concentration (C_o) of methylene blue dye with the concentration (C_t) after a certain period of time (t). Eqn. 9 was utilized to calculate the degradation removal (%) efficiency of methylene blue dye:

$$\eta = \frac{(C_t - C_o)}{C_t} \times 100 \quad (9)$$

Electrical conductivity of TiO_2-PMA nanocomposites: The electrical conductivity of both pure TiO_2 and TiO_2 doped phosphomolybdic acid (0.05 M) nanocomposite was studied by using two-probe methods with an LCR meter (Agilent 4284A). This technique involved two probes that was in contact with the material and the current passing between them. The frequency range was explored from 100 Hz to 1 MHz and the temperature range 303 to 393 K. The electrical conductivity of pure TiO_2 and TiO_2 doped phosphomolybdic acid nanocomposite, a sample powder was prepared by grinding the sample in a mortar and then 10% weight of polyvinyl alcohol was added as a binder. The mixture was subsequently compressed into discs of 11 mm diameter and 3 mm thickness under the pressure of 260 MPa to obtain a uniform shape and size of the pellets. An Agilent 4284A Precision LCR Meter was used to measure the electrical conductivity. Each sample was placed between two blocking electrodes with a diameter of 2.5 cm under spring pressure. The two-probe method was not only used to measure the both in AC and DC modes, but also provided the opportunity to measure the conductivity of the samples in a wide range of temperatures and frequencies.

Antimicrobial activity: The *Streptococcus pyogenes* (MTCC 442) bacterial strain was procured from HiMedia Lab. Pvt. Ltd., Mumbai, India. After culturing the bacterial strain in Mueller Hinton broth liquid medium at 33 ºC for 2 h with 200 rpm stirring, the antimicrobial activity of TiO_2-doped phosphomolybdic acid nanocomposites was assessed by the standard disk diffusion method. After incubating TiO_2 nanocomposite for 48 h, nutrient agar plates were separately moistened with bacterial suspensions of *Streptococcus pyogenes*. Whatman filter paper No.1 and discs of 20 mm diameter were impregnated with a 20 µL solution of TiO_2-doped phosphomolybdic acid nanocomposite in DMSO. After air-drying the discs, they were placed on the agar plates. Amoxicillin and potassium clavulanate were used as a positive control against bacteria and fungi respectively, while DMSO served as the negative control. Following that, the bacterial cultures were incubated at 37 ºC, while the fungus was incubated at 33 ºC for 48 h. The diameter of the inhibition ring, which indicated the activity zones of bacterial and nanocomposite growth, were evaluated.

RESULTS AND DISCUSSION

UV-Vis spectral studies: The UV-Vis spectra of sample 1 (pure TiO_2) and samples 2-5 [(TiO_2 doped phosphomolybdic acid (0.01 M, 0.001 M, 0.05 M and 0.005 M)] are shown in Fig. 1. The UV-Vis spectra of sample 1 showed a broad peak in the UV region, whereas samples 2 to 5 showed shifts in the peak positions and intensities. This is due to the presence of the dopants, which can modified the optical properties of the TiO_2 nanocomposite [16].

FTIR spectral studies: The FTIR spectra of the nanocomposites materials are shown in Fig. 2. Inthe FTIR spectra of sample 1, the key absorptions were observed at 3420, 2919, 1623, 1379 and 625 cm^{-1}, whereas samples 2 to 5 revealed the key frequency at 3478, 2927, 1640, 1374 and 675 cm^{-1}. These frequencies are attributed to various functional groups, such as stretchings of Ti-O-Ti, P-O and bending of Ti-O-P. The peak at 3478 cm^{-1} is related to the stretching vibration of hydroxyl group, whereas the frequency at 1640 cm^{-1} is attributed to the stretching vibration of the Ti-O-P frequency. The presence of the active frequency across all samples confirmed the formation of the nanocomposite. The broadness of the frequency indicated that the nanocomposite is of high purity. The peak intensities of all the frequency are comparable to each other [17-19].

XRD spectral studies: The XRD patterns of the TiO_2-PMA nanocomposites are shown in Fig. 3. The XRD pattern of pure TiO_2 consists of eight distinct peaks, which are characteristic of the TiO_2 crystalline structure (Table-1). The relative intensities of the peaks are in agreement with the theoretical values for TiO_2, confirming the presence of TiO_2 sample. The high crystallinity of the TiO_2 sample is evidenced by the sharpness of the peaks as well as the low background noise. Furthermore, the interplanar spacings for the TiO_2 peaks correspond with the theoretical values, indicating that the sample is of high purity. Sample 2-5 show the prominent peaks at 2θ of 26.1º, 27.8º, 35.8º, 39.1º, 40.9º, 54.1º, 56.2º, 62.2º and 68.8º corresponding to the (100), (002), (112), (020), (120), (202), (214), (032) and (132) planes, respectively. These peaks indicate the crystal structure of TiO_2 to be predominantly anatase with a few minor rutile phases [20-22]. The doping of phosphomolybdic acid causes significant change in the peak positions or intensity indicating the crystal structure to be affected by doping. The presence of phosphomolybdic acid nanocomposite in TiO_2 nanocomposites can be confirmed by comparing the peak positions with the JCPDS file no. 89-6975.

SEM and EDAX studies: Scanning electron microscopy (SEM) coupled with energy dispersive spectrometry (EDAX) analysis was used to investigate the nanostructures of the pure TiO_2 and TiO_2-doped phosphomolybdic acid nanocomposites. The SEM image (Fig. 4a) revealed that pure TiO_2 is spherical

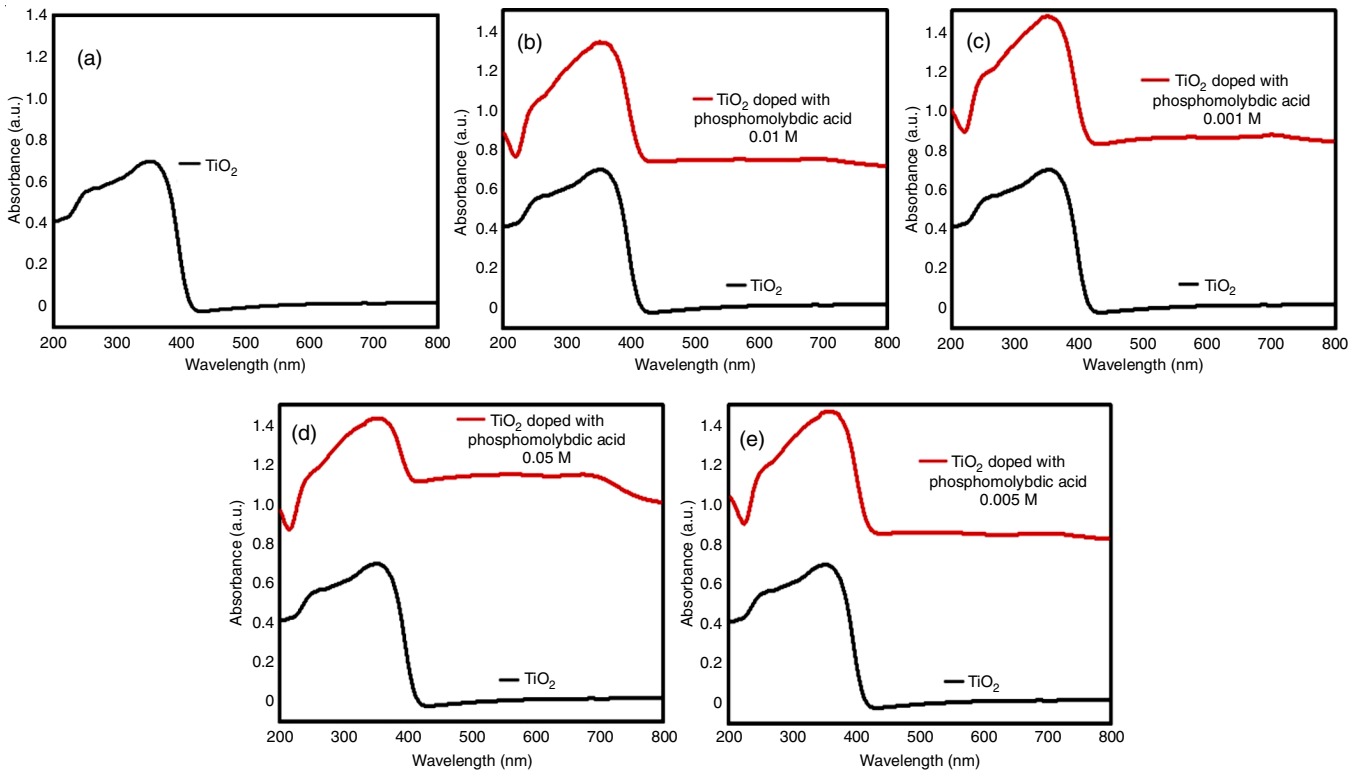

Fig. 1. UV-Visible spectrum of TiO_2 and TiO_2 doped with phosphomolybdic acid nanocomposite

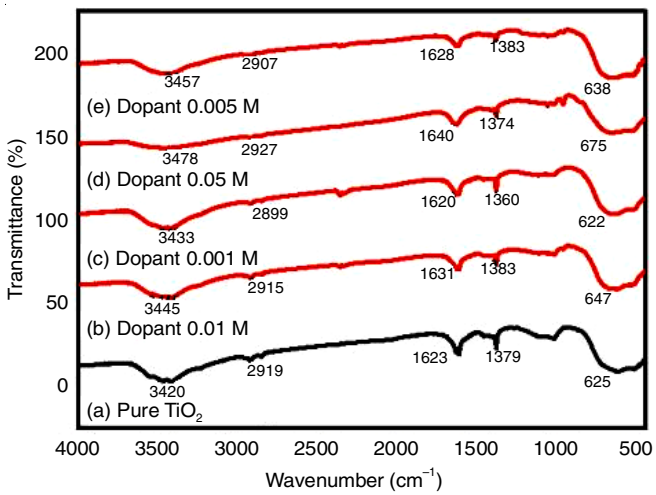

Fig. 2. FTIR spectra of TiO_2 doped phosphomolybdic acid nanocomposites

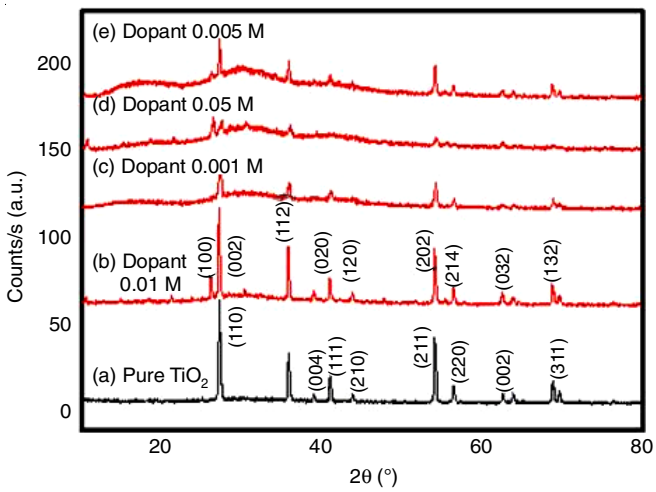

Fig. 3. XRD spectrum of phosphomolybdic acid doped TiO_2 nanocomposites

in shape and had an average particle size. The EDAX spectra of sample 1 showed that it contained only titanium, for the pure TiO_2. The SEM images of samples 2 to 5 (Fig. 4b-e) showed that the TiO_2 particles were well dispersed in the phosphomolybdic acid matrix. The EDAX spectra of these samples revealed the presence of titanium, phosphorus and molybdenum, indi-

TABLE-1
THE XRD DATA OF PURE TiO_2 AND TiO_2-PHOSPHOMOLYBDIC ACID NANOCOMPOSITES

Nanocomposites	Parameters		Peak position	FWHM	Intercept	Average crystallite size	Slope	d-spacing (Å)	Average d-spacing (Å)
	K	λ (Å)	2θ (?)	β (°)	c = kλ/D	D (nm)	m	$d_{hkl} = \lambda/(2 \sin \theta)$	
TiO_2	0.94	1.5406	27.14	0.2775	0.0037	29.63	0.0004	3.28	1.99
TiO_2 + PMA 0.010 M	0.94	1.5406	26.10	0.2344	0.0051	25.26	0.0009	3.41	2.47
TiO_2 + PMA 0.001 M	0.94	1.5406	27.22	0.4041	0.0089	14.33	0.0015	3.27	1.98
TiO_2 + PMA 0.050 M	0.94	1.5406	26.35	0.3862	0.0062	11.75	0.0013	3.37	2.55
TiO_2 + PMA 0.005 M	0.94	1.5406	17.69	7.8267	0.0066	5.28	0.0002	5.00	2.45

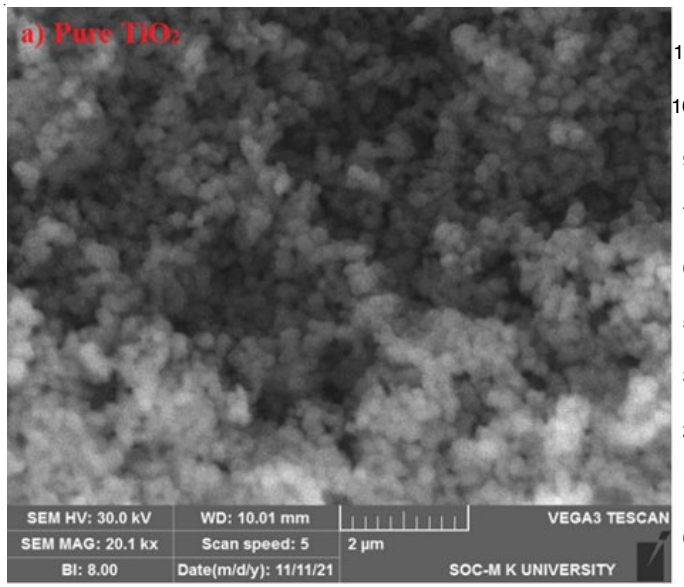

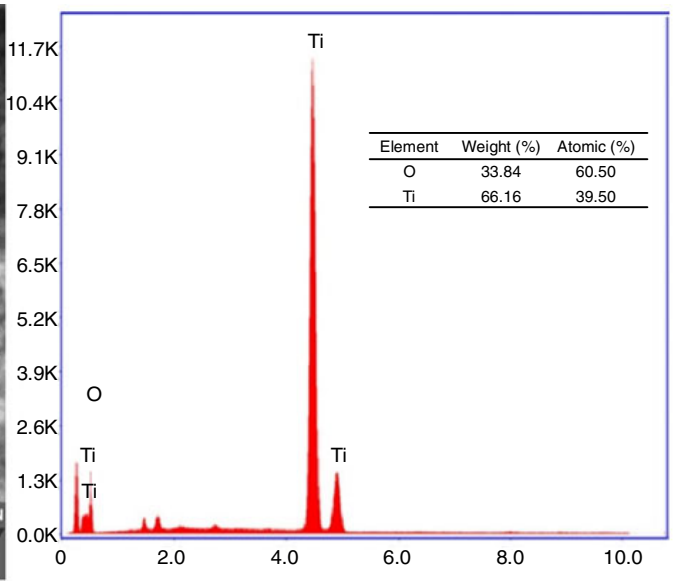

Element	Weight (%)	Atomic (%)
O	33.84	60.50
Ti	66.16	39.50

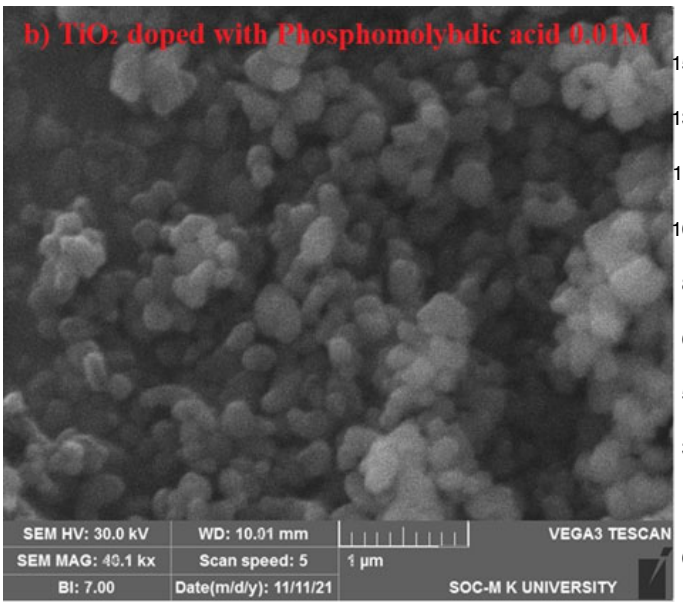

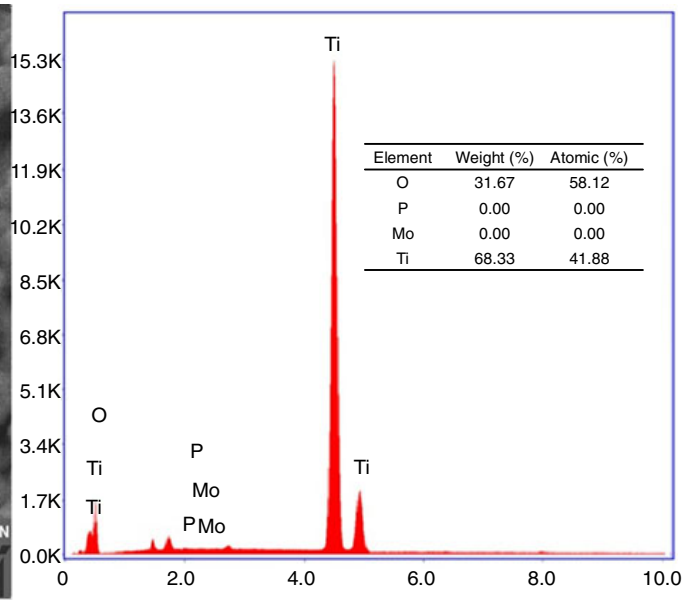

Element	Weight (%)	Atomic (%)
O	31.67	58.12
P	0.00	0.00
Mo	0.00	0.00
Ti	68.33	41.88

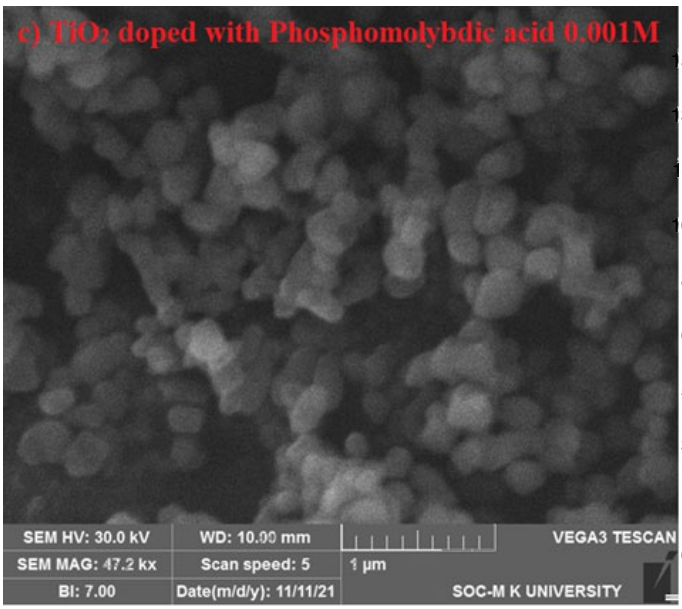

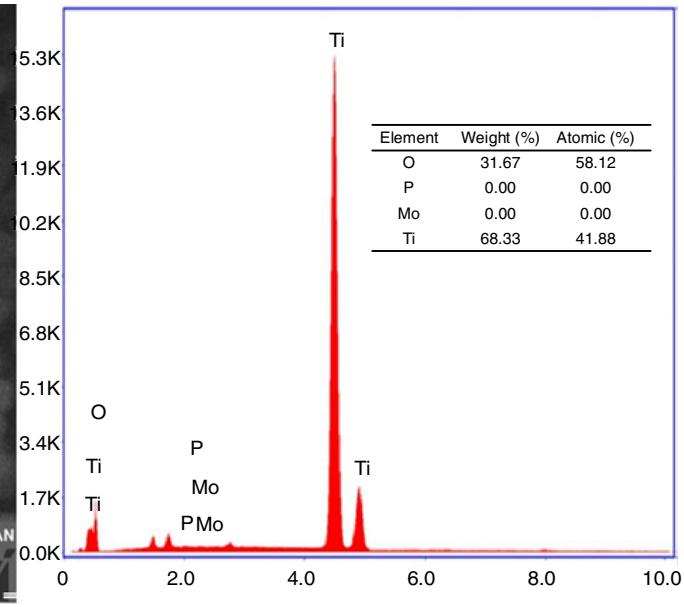

Element	Weight (%)	Atomic (%)
O	31.67	58.12
P	0.00	0.00
Mo	0.00	0.00
Ti	68.33	41.88

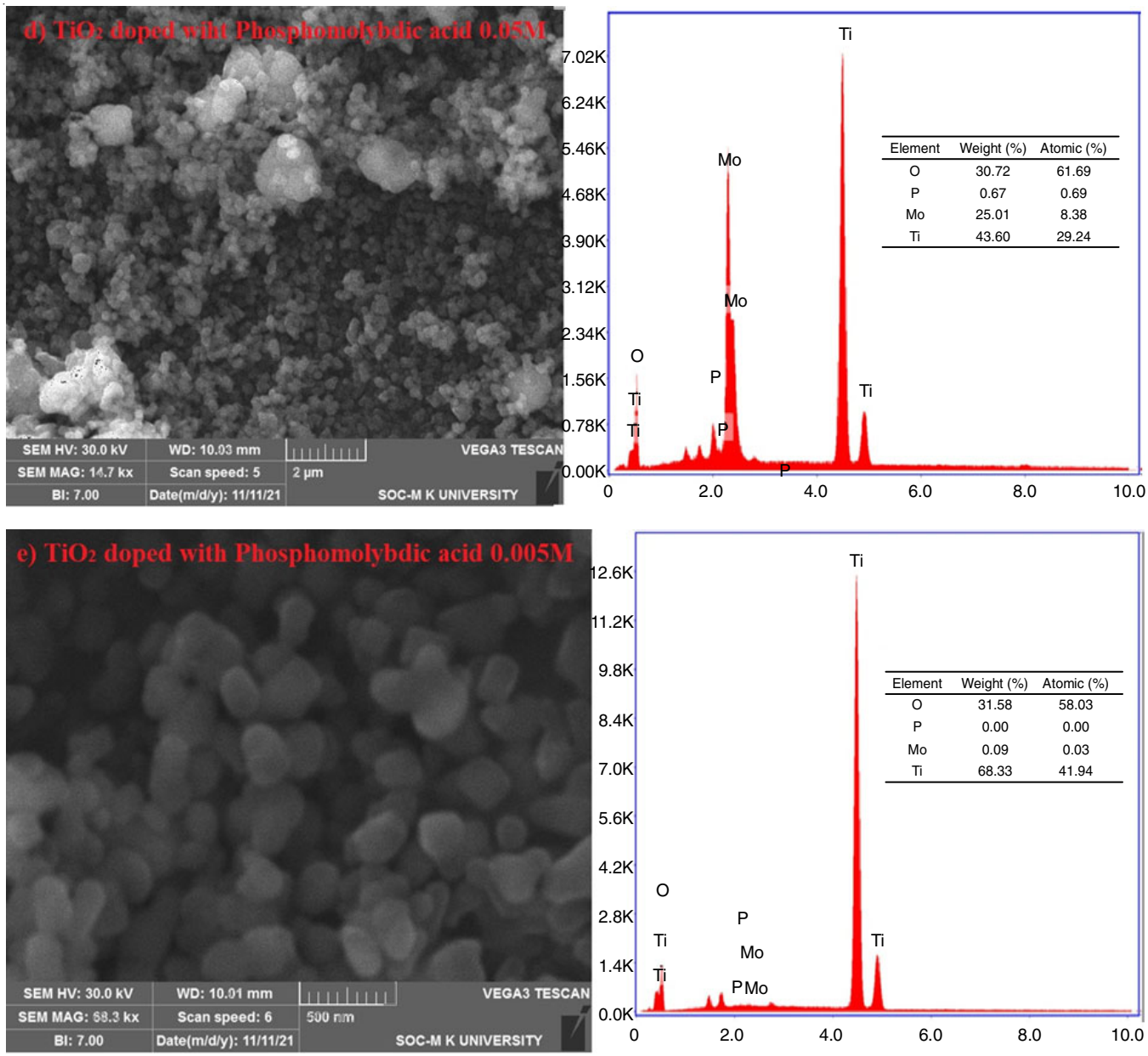

Fig. 4. SEM and EDAX of pure TiO_2 and TiO_2 doped with phosphomolybdic acid nanocomposites

cating a successful doping of TiO_2 into the phosphomolybdic acid. Furthermore, the nanocomposites had an average particle size of around 100 nm, which is larger than that of pure TiO_2. This result suggested that doping of TiO_2 into the phosphomolybdic acid matrix had a considerable effect on the particle size of the nanocomposites [23,24].

Average particle: The average particle size of the samples [25-27] were analyzed by using ImageJ, as shown in Fig. 5. Sample 1 is composed of pure TiO_2, which had an average particle size of 0.15 nm. The remaining samples 2 to 5 average particle sizes of 0.23, 0.22, 0.15 and 0.32 nm, respectively. The particle size of the nanocomposites are significantly larger than that of pure TiO_2, illustrating the impact of the doping process on the structure of the particles. The larger particles are likely the results of increased interparticle interactions due to the addition of the phosphomolybdic acid, which could lead to agglomeration of the particles. The enhanced particle size may also facilitate improved dispersion of the nanocomposites in various polymers, resulting in improved mechanical and optical properties. Thus, doping of TiO_2 with phosphomolybdic acid can be used to tailor the particle size of the nanocomposites for specific applications.

Photocatalytic studies

Photodegradation of methylene blue dye: The photodegradation of methylene blue dye [28] was carried out by using a nanocomposite as photocatalyst. The initial concentration of the dye was optimized at 50 mg/L having a catalyst dosage of 0.5 g/L. The wavelength used for photodegradation was 365 nm and the O.D of degraded sample was absorbed at 460 nm. Under these conditions, the nanocomposite was able to achieve maximum 99.41% degradation of dye (Fig. 6).

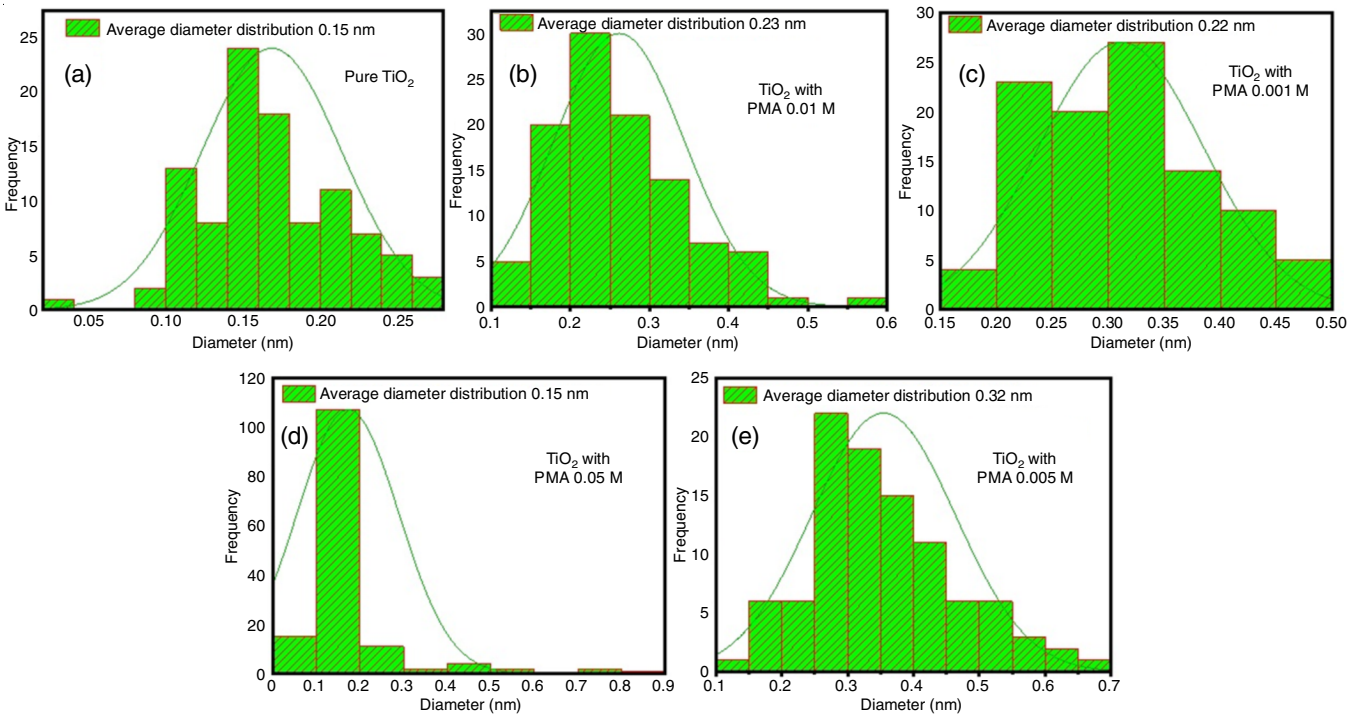

Fig. 5. Average diameter analysis of pure TiO_2 and TiO_2 doped phosphomolybdic acid nanocomposites

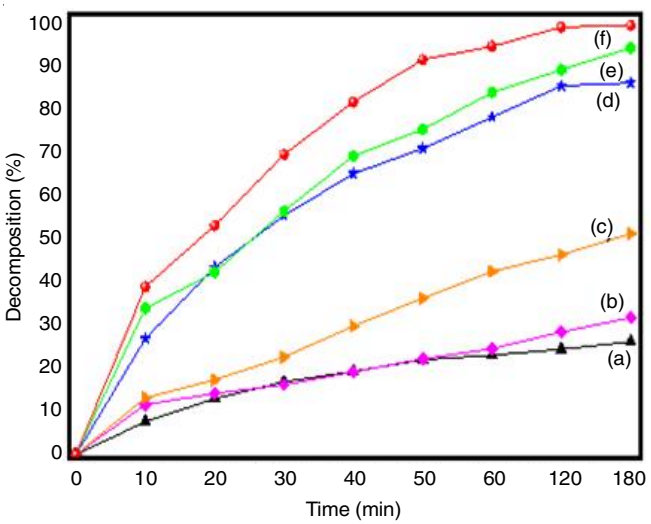

Fig. 6. Phosphomolybdic acid photocatalyst concentration variation (a) 10 mg, (b) 20 mg, (c) 50 mg, (d) 100 mg, (e) 125 mg and (f) 150 mg [Condition: methylene blue = 50 mg/L; temp. = 33 °C; without airflow and photodegradation wavelength = 365 nm and O.D. measured at λ_{max} = 460 nm]

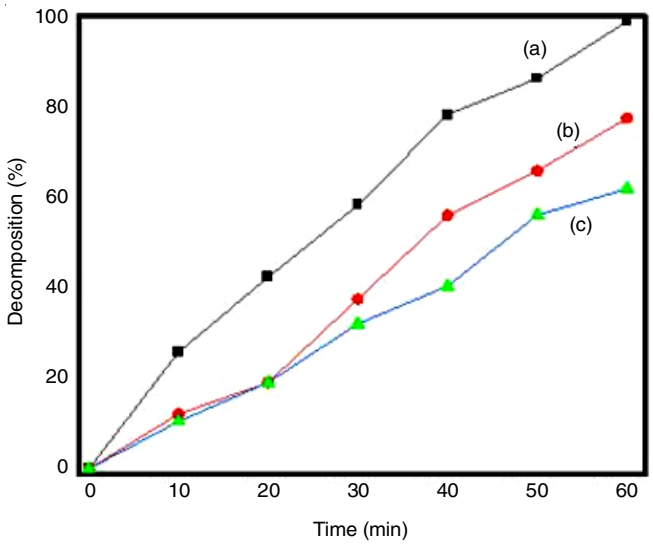

Fig. 7. Effect of pH variation on photodegradation of methylene blue (a) 4, (b) 6 and (c) 8 [Condition: methylene blue = 50 mg/L; temp. = 33 °C; catalyst dose = 0.5 g/L and photodegradation wavelength =365 nm]

Effect of pH on photocatalytic degradation of methylene blue: The study of the photocatalytic degradation of methylene blue at different pH values were conducted to investigate the effect of pH on the process. A solution of methylene blue with a concentration of 50 mg/L was mixed with 0.5 g/L of catalyst and exposed to UV radiation at 365 nm. The pH of the solution was adjusted to 4, 6 and 8 by adding 0.1 M of HCl and NaOH. After 60 min, the degradation efficiency was found as 98.82%, 77.46% and 63.19%, respectively (Fig. 7). The highest degradation rate was observed at pH 4 and the lowest at pH 6 and 8. This is likely due to the fact that when the pK_a of the methylene blue was relatively high and at lower pHs, the availability of the aromatic ring in the solution is increased, thus providing the optimum conditions for the photocatalytic degradation of the molecules [29-31]. The results of the study suggest that pH plays an important role in the process, with the rate of degradation decreasing with increased pH. Therefore, the pH of the solution should be adjusted to 4 in order to obtain the best results.

Effect of demineralization: Demineralization is the process of removing minerals from water, which can be done through photocatalysis. Photocatalysis involves the absorption of ultraviolet light by dye molecules, which then generates reactive

oxygen species that can oxidize methylene blue dye. To determine the demineralization efficiency of methylene blue dye, it was subjected to optimized conditions, including dye concentration of 50 mg/L was mixed with 0.5 g/L, pH of 4 and wavelength of 365 nm at 33 ºC for the photodegradation. After 4 h, the results showed that the dye was completely demineralized 99.81% (Fig. 8).

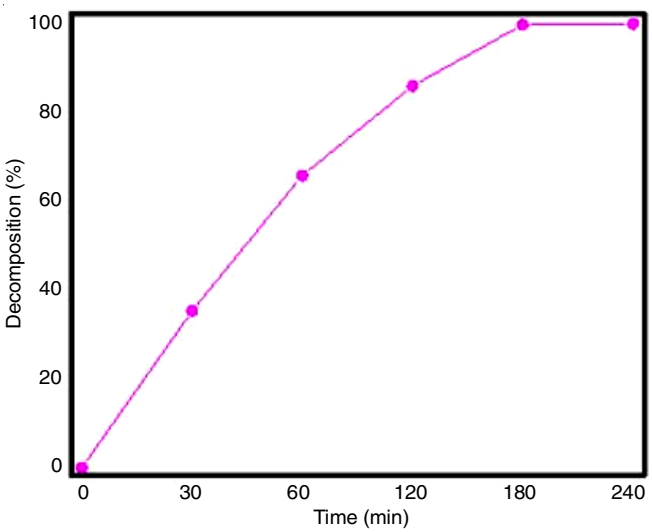

Fig. 8. Effect of demineralization of methylene blue dye [Condition: methylene blue = 50 mg/L; temp. = 33 °C; catalyst dose = 0.5 g/L and photodegradation wavelength = 365 nm]

Electrical conductivity studies by two probe method: The results of the doping of TiO_2 with phosphomolybdic acid nanocomposite of 0.05 M PMA can significantly improve the electrical conductivity of the material. The conductivity of the doped sample being higher than that of the pure TiO_2 sample. Furthermore, the conductivity of the doped sample increased when the frequency was increased from 100 Hz to 1 MHz, indicating a frequency-dependent response. This can be attributed to the doping of sample with the phosphorus-molybdenum complex, which acts as an electron donor, increasing the number of available charge carriers and the electrical conductivity [32].

AC conductivity studies: The electrical conductivity measurements by two probe methods are shown in Fig. 9. The AC conductivity of pure TiO_2 and TiO_2 doped phosphomoly-bdic acid nanocomposites were studied at different temperatures (303, 333, 363 and 393 K). The electrical properties of pure TiO_2 increased with temperature. This is because the thermal energy at higher temperatures allows for more charge carriers to be activated, which increases the conductivity. The electrical properties of TiO_2 doped phosphomolybdic acid also increased with temperature. However, the increase was more than for pure TiO_2. This is because the phosphomolybdic acid dopant acts as a trap for charge carriers, which increases the number of available charge carriers at higher temperatures [33,34].

In addition, a comparison between the electrical conductivity of pure TiO_2 and TiO_2 doped phosphomolybdic acid nanocomposites has revealed that TiO_2 doped PMA exhibits a much greater electrical conductivity. This increase in electrical conductivity is attributed to the presence of molybdenum and phosphorus in the phosphomolybdic acid-doped nanocomposites, which increase the number of conduction pathways for charge carriers thus increasing the electrical conductivity.

DC conductivity studies: In Fig. 10, the electrical conductivity tests of TiO_2 and TiO_2-phosphomolybdic acid nanocomposites were conducted using two-probe techniques at 33 ºC and 0 to 400 volts. The results showed that the electrical conductivity of pure TiO_2 increased slowly at first, but then increased steeply at higher voltages. This is because the voltage applied to the sample created an electric conduction, which caused the free electrons in the TiO_2 lattice to move. However, the movement of the free electrons was initially hindered by the defects in the TiO_2 lattice. At higher voltages, the electric field was strong enough to overcome the defects in the lattice, allowing the free electrons to move more freely. This is because the number of localized states in the bandgap of TiO_2 increases with increasing phosphomolybdic acid concentration. This leads to an increase in the number of charge carriers available for conduction, which increases the electrical conductivity. The combination of these two effects results in a significant increase in the electrical conductivity of TiO_2-doped phosphomolybdic acid [35,36].

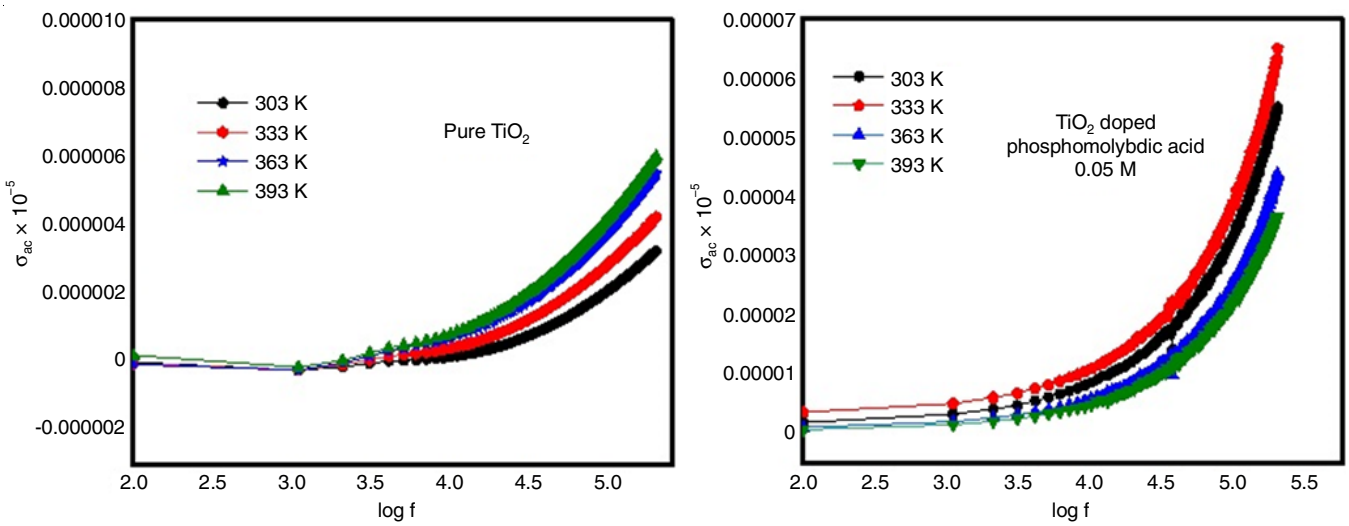

Fig. 9. Frequency-dependent AC of pure TiO_2 and TiO_2 doped phosphomolybdic acid (0.05 M) nanocomposites at varying temperatures

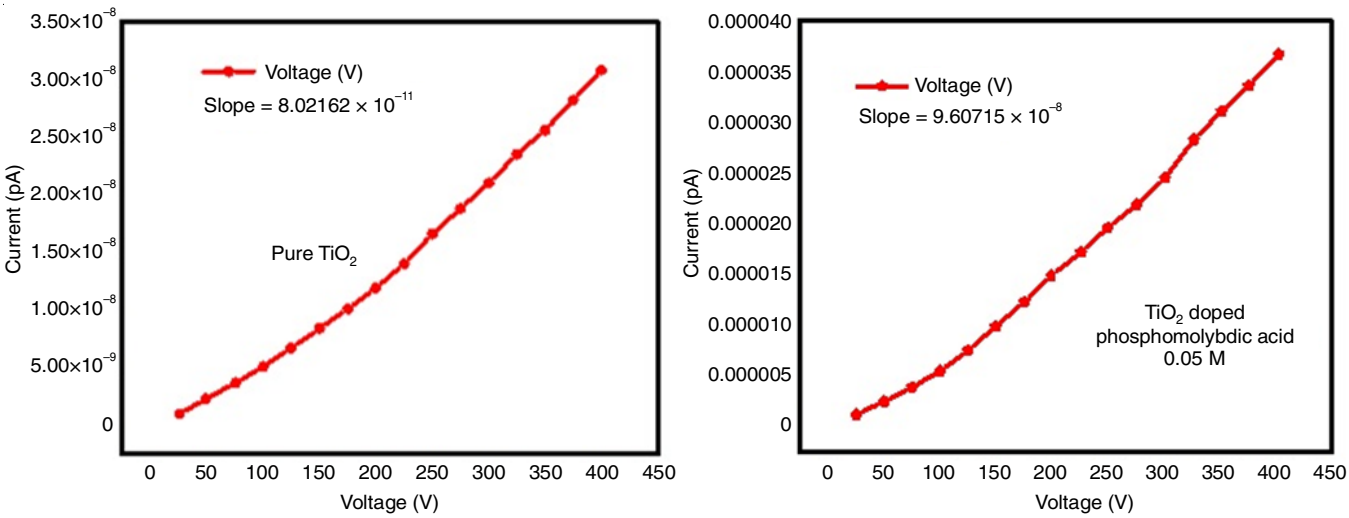

Fig. 10. DC conductivity of pure TiO_2 and TiO_2 doped with phosphomolybdic acid (0.05 M) nanocomposite

Dielectric studies: The dielectric constant and electrical conductivity of pure TiO_2 and TiO_2 doped phosphomolybdic acid were investigated at 303, 333, 363 and 393 K. The results showed that the dielectric constant of both materials gradually increased slowly with temperature (Fig. 11). This is because the thermal energy at higher temperatures allows for more molecular dipoles to apply an electric field, resulting in a higher dielectric constant. The electrical conductivity of pure TiO_2 was also found to increase with temperature but at a slower rate than the dielectric constant. This is because the electrical conductivity is also affected by the mobility of charge carriers. The doping of TiO_2 with phosphomolybdic acid resulted in a significant increase in both dielectric constant and electrical conductivity. This is because phosphomolybdic acid is a strong electron donor, which increases the number of free electrons in the TiO_2 matrix. These free electrons contribute to the electrical conductivity, while also increasing the polarizability of the TiO_2 matrix, which leads to a higher dielectric constant [37].

The dielectric loss and electrical conductivity of TiO_2-doped phosphomolybdic acid were found to be significantly higher than the dielectric loss and electrical conductivity of pure TiO_2 (Fig. 12). The dielectric loss of pure TiO_2 increases with decreasing temperature and this pattern shows a strong linear relationship. The electrical conductivity of TiO_2-doped phosphomolybdic acid nanocomposites usually increases with increasing temperature, but when the temperature exceeds 363 K the electrical conductivity decreases. The doping of TiO_2 with phosphomolybdic acid has two main effects on dielectric loss and electrical conductivity. First, it increases the number of oxygen vacancies in the crystal structure. Since, phosphomolybdic acid is a Lewis acid and it can react with the oxygen atoms in TiO_2 to form oxygen vacancies, secondly, phosphomolybdic acid can also act as a charge carrier. This is because it has a relatively high ionic conductivity. The combined effect of these two factors is to increase the dielectric loss and electrical conductivity of TiO_2- phosphomolybdic acid.

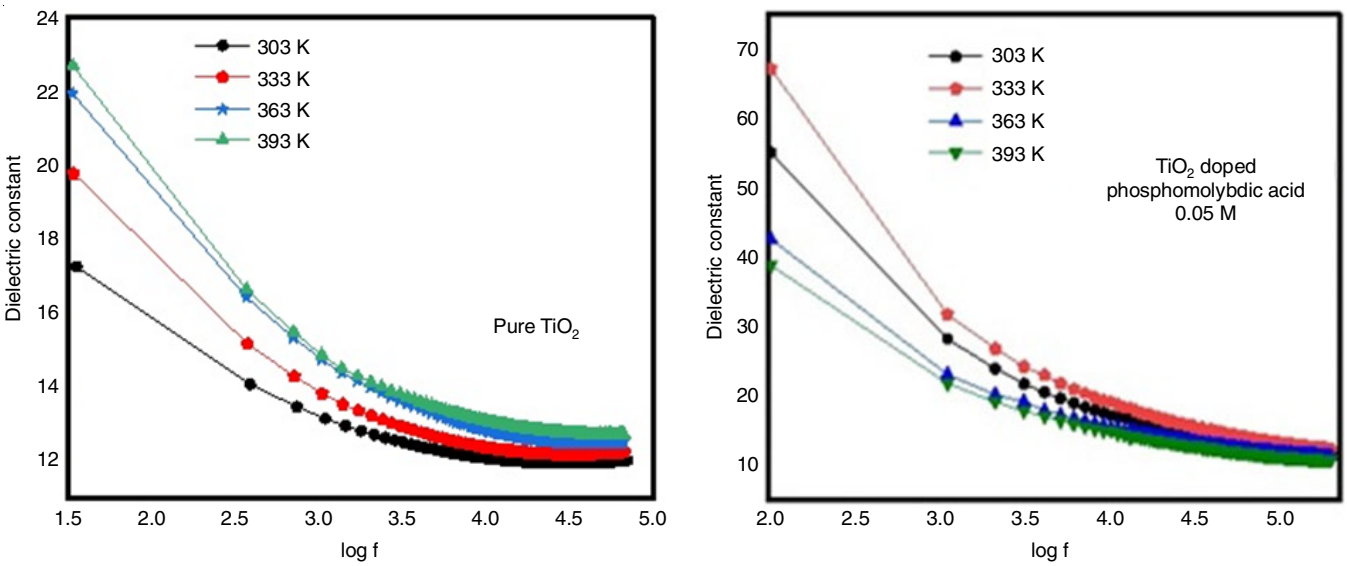

Fig. 11. Frequency-dependent dielectric constant for pure TiO_2 and TiO_2 doped phosphomolybdic acid nanocomposites at varying temperatures

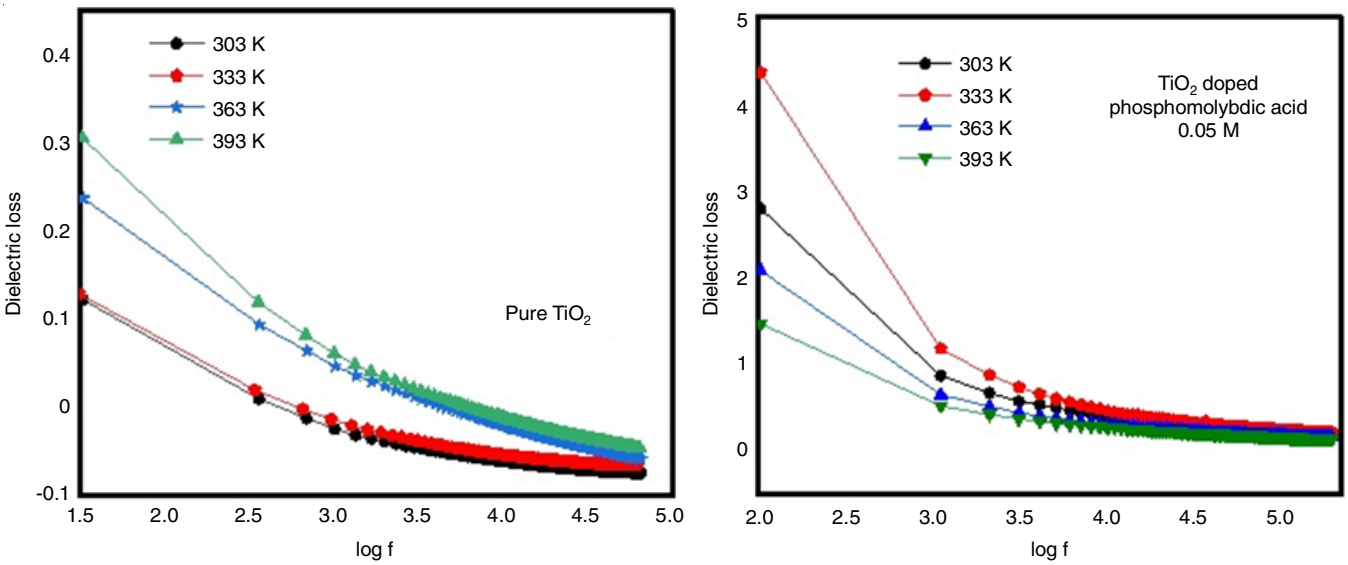

Fig. 12. Frequency-dependent dielectric loss for pure TiO_2 and TiO_2 doped phosphomolybdic acid nanocomposites at varying temperatures

Antimicrobial activity: The combination of amoxicillin and potassium clavulanate has been widely used in the treatment of infections caused by *Streptococcus pyogenes* bacteria, a common cause of dental caries. Furthermore in evaluate the antimicrobial activity of this antibiotic combination, a disc diffusion method was used using TiO_2-doped phosphomolybdic acid nanocomposite. The nanocomposite was dissolved in DMSO solvent and then applied to filter paper discs, which were then placed on the agar plates containing the *Streptococcus pyogenes* bacteria. Following an incubation period of 48 h at 37 ºC, the inhibitory effect of the nanocomposite was assessed by measuring the diameter of the zone of inhibition around the paper discs. The results showed that TiO_2-doped phosphomolybdic acid nanocomposite had a potent antimicrobial effect against *Streptococcus pyogenes* bacteria, with a significantly larger zone of inhibition around the discs containing the nanocomposite than that of the control discs (Fig. 13). Moreover, the combination of amoxicillin and potassium clavulanate displayed a stronger antimicrobial activity than the nanocomposite on its own, suggesting that the two antibiotics synergistically enhanced the antimicrobial activity of the nanocomposite. Consequently, the disc diffusion method, using TiO_2-doped phosphomolybdic acid nanocomposite combined with amoxicillin and potassium clavulanate, demonstrated a potent antimicrobial effect against *Streptococcus pyogenes* bacteria, making it a promising treatment option for infections caused by this particular bacteria. Thus, this combination of two antibiotics with the nanocomposite could be a beneficial therape-

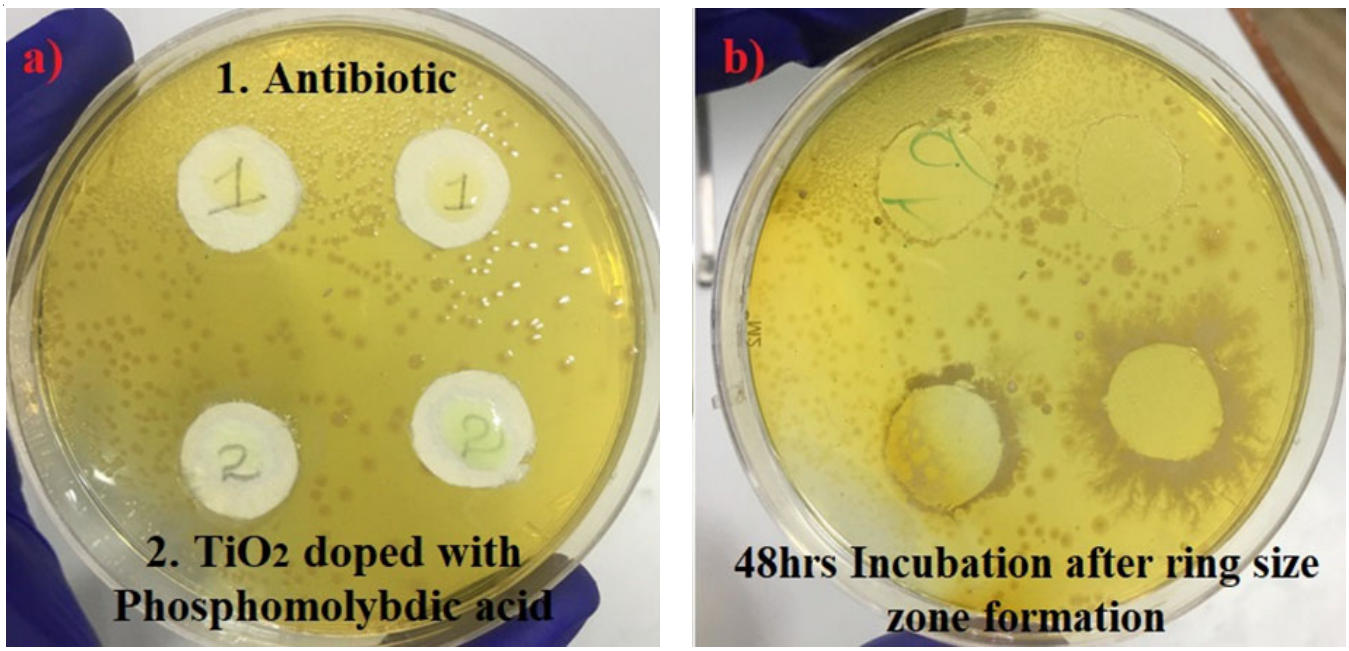

Fig. 13. Antimicrobial activity TiO_2 doped phosphomolybdic acid nanocomposites

utic approach for treating infections caused by this bacterium [38,39].

Conclusion

TiO_2 doped with various concentration of phosphomolybdic acid nanocomposites were synthesized by annealing method and characterized by UV-vis, FTIR, XRD, SEM and EDX techniques. The UV-Vis and FTIR showed strong interaction between TiO_2 and PMA. XRD, SEM and EDX revealed that when PMA was added, there was a shift in peak position, decreases of crystallinity, decreases of particle size and uniform distribution of dopant into the TiO_2 matrix. In photocatalysis, the preliminary experiment confirmed the essential of light and catalyst for the degradation of methylene blue dye. The established optimal condition was at pH 4 with [methylene blue] = 50 ppm; temperature = 33 ºC, catalyst dose = 0.05 M and at the photodegradation wavelength of 365 nm, TiO_2-PMA exhibited the maximum degradation efficiency of 99.58%. The disc diffusion method, TiO_2-PMA composite combined with amoxicillin and potassium clavulanate, demonstrated a potent antimicrobial effect against *Streptococcus pyogenes* bacteria, making it a promising treatment option for infection caused by this particular bacterial. Furthermore, it was observed that the TiO_2-PMA composite exhibited AC and DC conductivities, which increases with increase in temperature and frequencies.

ACKNOWLEDGEMENTS

The authors are thankful to the Department of Chemistry & Zoology, St. John's College, Palayamkottai, India for providing the necessary facilities to conduct the experiments.

CONFLICT OF INTEREST

The authors declare that there is no conflict of interests regarding the publication of this article.

REFERENCES

1. R.J. Sengwa and P. Dhatarwal, *Opt. Mater.*, **113**, 110837 (2021); https://doi.org/10.1016/j.optmat.2021.110837
2. R. Anand, B.B. Nayak and S.K. Behera, *Ceram. Int.*, **47**, 27822 (2021); https://doi.org/10.1016/j.ceramint.2021.06.210
3. T.H. AlAbdulaal and I.S. Yahia, *Optik*, **227**, 166036 (2021); https://doi.org/10.1016/j.ijleo.2020.166036
4. R. Magaña-López, P.I. Zaragoza-Sánchez, B.E. Jiménez-Cisneros and A.C. Chávez-Mejía, *Water*, **13**, 1641 (2021); https://doi.org/10.3390/w13121641
5. N. Torkian, A. Bahrami, A. Hosseini-Abari, M.M. Momeni, M. Abdolkarimi-Mahabadi, A. Bayat, P. Hajipour, H. Amini Rourani, M.S. Abbasi, S. Torkian, Y. Wen, M. Yazdan Mehr and A. Hojjati-Najafabadi, *Environ. Res.*, **207**, 112157 (2022); https://doi.org/10.1016/j.envres.2021.112157
6. S.H. Ammar, W.A. Abdulnabi and H.D.A. Kader, *Environ. Nanotechnol. Monit. Manag.*, **13**, 100289 (2020); https://doi.org/10.1016/j.enmm.2020.100289
7. M.S. Lakshmi, S.M. Wabaidur, Z.A. Alothman, M.R. Johan, V.K. Ponnusamy and R. Dhanusuraman, *Int. J. Energy Res.*, **45**, 8243 (2021); https://doi.org/10.1002/er.5950
8. A.M. Escobar, G. Blustein, R. Luque and G.P. Romanelli, *Catalysts*, **11**, 291 (2021); https://doi.org/10.3390/catal11020291
9. Z. Chengli, M. Ronghua, W. Qi, Y. Mingrui, C. Rui and Z. Xiaonan, *J. Coord. Chem.*, **74**, 1751-1764 (2021); https://doi.org/10.1080/00958972.2021.1940982
10. S.R. Yousefi, H.A. Alshamsi, O. Amiri and M. Salavati-Niasari, *J. Mol. Liq.*, **337**, 116405 (2021); https://doi.org/10.1016/j.molliq.2021.116405
11. A. Nikoonahad, B. Djahed, S. Norzaee, H. Eslami, Z. Derakhshan, M. Miri, Y. Fakhri, E. Hoseinzadeh, S.M. Ghasemi, D. Balarak, R.A. Fallahzadeh, M. Zarrabi and M. Taghavi, *PeerJ.*, **6**, e5501 (2018); https://doi.org/10.7717/peerj.5501
12. L. Da Silva Mathias, J.C. De Aquino Almeida, L.C. Passoni, C.M. D. Gossani, G.B. Taveira, V.M. Gomes and O. Vieira-Da-Motta, *J. Microbiol. Biotechnol.*, **30**, 540 (2020); https://doi.org/10.4014/jmb.1907.07064
13. Y. Wei, B. Han, Z. Dong and W. Feng, *J. Mater. Sci. Technol.*, **35**, 1951 (2019); https://doi.org/10.1016/j.jmst.2019.05.014
14. Z. Huang, Z. Yang, M.Z. Hussain, Q. Jia, Y. Zhu and Y. Xia, *J. Mater. Sci. Technol.*, **84**, 76 (2021); https://doi.org/10.1016/j.jmst.2020.12.057
15. Z.H. Mahmoud, R.A. AL-Bayati and A.A. Khadom, *J. Oleo Sci.*, **71**, 311 (2022); https://doi.org/10.5650/jos.ess21283
16. Z. Man, Y. Meng, X. Lin, X. Dai, L. Wang and D. Liu, *Chem. Eng. J.*, **431**, 133952 (2022); https://doi.org/10.1016/j.cej.2021.133952
17. K. Divakaran, A. Baishnisha, V. Balakumar, K.N. Perumal, C. Meenakshi and R.S. Kannan, *J. Environ. Chem. Eng.*, **9**, 105560 (2021); https://doi.org/10.1016/j.jece.2021.105560
18. B. Al-saida, W.A. Amer, E.E. Kandyel and M.M. Ayad, *J. Photochem. Photobiol. Chem.*, **392**, 112423 (2020); https://doi.org/10.1016/j.jphotochem.2020.112423
19. H.M. El-Sharkawy, A.M. Shawky, R. Elshypany and H. Selim, *Sci. Rep.*, **13**, 8845 (2023); https://doi.org/10.1038/s41598-023-35265-7
20. G.H. Jetani and M.B. Rahmani, *Eur. Phys. J. Plus*, **135**, 720 (2020); https://doi.org/10.1140/epjp/s13360-020-00739-4
21. A. Ahmed, A. Singh, A. Sharma, S. Prerna, S. Verma, S. Mahajan and S. Arya, *Solid State Sci.*, **116**, 106617 (2021); https://doi.org/10.1016/j.solidstatesciences.2021.106617
22. M.V. Arularasu, M. Harb and R. Sundaram, *Carbohydr. Polym.*, **249**, 116868 (2020); https://doi.org/10.1016/j.carbpol.2020.116868
23. R.A. Talib, D.K. Thbayh and K.A. Mohammed, *Mater. Sci. Forum*, **1065**, 101 (2022); https://doi.org/10.4028/p-s6y8z3
24. A. Tiwari, A. Shukla, D. Lalliansanga, D. Tiwari and S.M. Lee, *Environ. Technol.*, **41**, 3500 (2020); https://doi.org/10.1080/09593330.2019.1615127
25. P.K. Boruah and M.R. Das, *J. Hazard. Mater.*, **385**, 121516 (2020); https://doi.org/10.1016/j.jhazmat.2019.121516
26. N.A. Ahir, A.V. Takaloo, K.A. Nirmal, S.S. Kundale, M.Y. Chougale, J. Bae, D. Kim and T.D. Dongale, *Mater. Sci. Semicond. Process.*, **125**, 105646 (2021); https://doi.org/10.1016/j.mssp.2020.105646
27. M. Vedhanayagam, S. Anandasadagopan, B.U. Nair and K.J. Sreeram, *Mater. Sci. Eng. C*, **108**, 110378 (2020); https://doi.org/10.1016/j.msec.2019.110378
28. T.Q.Q. Viet, V.H. Khoi, N.T.H. Giang, H.T.V. Anh, N.M. Dat, M.T. Phong and N.H. Hieu, *Colloids Surf. A Physicochem. Eng. Asp.*, **629**, 127464 (2021); https://doi.org/10.1016/j.colsurfa.2021.127464
29. Z. Siraj, I.M. Maafa, I. Shafiq, N. Shezad, P. Akhter, W. Yang and M. Hussain, *Environ. Sci. Pollut. Res. Int.*, **28**, 53340 (2021); https://doi.org/10.1007/s11356-021-14442-z
30. R. Priya, S. Stanly, S.B. Dhanalekshmi, F. Mohammad, W.C. Oh, H.A. Al-Lohedan and S. Sagadevan, *Optik*, **206**, 164281 (2020); https://doi.org/10.1016/j.ijleo.2020.164281
31. S.P. Santoso, A.E. Angkawijaya, V. Bundjaja, C.-W. Hsieh, A.W. Go, M. Yuliana, H.-Y. Hsu, P.L. Tran-Nguyen, F.E. Soetaredjo and S. Ismadji, *Int. J. Biol. Macromol.*, **193**, 721 (2021); https://doi.org/10.1016/j.ijbiomac.2021.10.044

32. B. Raghavendra, T. Sankarappa and A. Malge, *J. Inorg. Organomet. Polym.*, **32**, 2416 (2022); https://doi.org/10.1007/s10904-022-02358-1
33. K. Suhailath and M. Ramesan, *J. Thermoplast. Comp. Mater.*, **33**, 1061 (2020); https://doi.org/10.1177/0892705718817350
34. Q.A. Alsulami and A. Rajeh, *Results Phys.*, **28**, 104675 (2021); https://doi.org/10.1016/j.rinp.2021.104675
35. A. Husain, M.U. Shariq and F. Mohammad, *Materialia*, **9**, 100599 (2020); https://doi.org/10.1016/j.mtla.2020.100599
36. A. Husain, S. Ahmad and F. Mohammad, *Mater. Chem. Phys.*, **239**, 122324 (2020); https://doi.org/10.1016/j.matchemphys.2019.122324
37. A. Shubha, S.R. Manohara and B. Angadi, *Polym. Bull.*, **79**, 7117 (2022); https://doi.org/10.1007/s00289-021-03838-z
38. M. Mesgari, A.H. Aalami and A. Sahebkar, *Int. J. Biol. Macromol.*, **176**, 530 (2021); https://doi.org/10.1016/j.ijbiomac.2021.02.099
39. M.R. Amiri, M. Alavi, M. Taran and D. Kahrizi, *J. Public Health Res.*, **11**, 2 (2022); https://doi.org/10.1177/22799036221104151